Ionic Mechanisms in Secretagogue-induced Morphological Changes in Rat Parotid Gland

BARBARA A. LESLIE and JAMES W. PUTNEY, JR.
Departments of Anatomy and Pharmacology, Medical College of Virginia, Virginia Commonwealth University, Richmond, Virginia 23298

ABSTRACT When 10^{-5} M carbachol was added to parotid tissue slices incubated in buffer containing Ca^{++}, watery vacuoles were formed in the cells. The percent volume density of vacuoles, as measured from 0.5-μm sections, increased from 0.64 ± 0.15 SE (n = 7) to 3.09 ± 0.99 (n = 5) in 10 min and, finally, to 7.27 ± 1.88 (n = 4) in 30 min. In electron micrographs, most of the vacuoles appeared to arise from a location near the Golgi apparatus. Condensation of nuclear chromatin and a conformational change in mitochondria were also noted immediately after stimulation. The percent volume density values returned to basal levels with the addition of either 5 mM EGTA or 10^{-6} M atropine after the addition of carbachol. Nuclei and mitochondria returned to normal configurations.

In the presence of either 1 mM ouabain or high K^+, or in the absence of added Ca^{++}, carbachol failed to induce vacuole formation. However, low Na^+ medium did not prevent the formation of vacuoles due to carbachol. Ultrastructural changes in nuclei and mitochondria were consistently associated with the appearance of vacuoles. Since both high K^+ and ouabain blocked vacuole formation, it is unlikely that Na^+ or K^+ movements were important for the response. Rather, receptor-activated Ca^{++} influx, which is likely to be inhibited by depolarizing agents (such as high K^+ or ouabain), is probably the more important factor in vacuole formation and other concomitant ultrastructural changes.

A variety of exocrine glands, when stimulated to secrete, form watery vacuoles in the Golgi region of the cell. Although most extensively studied in the rat parotid gland (1, 2) a similar phenomenon has been noted for the submandibular gland (3), exocrine pancreas (4), and tracheal submucosal glands (5, 6). Vacuole formation is generally studied with in vitro preparations, but Garrett and Harrop (7) have shown vacuolation in the rat parotid gland on stimulation of the parasympathetic nerves in vivo. The mechanism and significance of this response are not known.

In the rat parotid gland, the receptors associated with vacuole formation (i.e., muscarinic-cholinergic, α-adrenergic), also regulate secretion of water and electrolytes, and are distinct from receptors (β-adrenergic) involved in zymogen secretion (1). The regulation of electrolyte secretion manifests itself in vitro as alterations in cellular content of Na^+ and K^+ (8). The changes in cellular Na^+ and K^+ induced by cholinergic stimuli are Ca^{++}-dependent and it has been suggested that Ca^{++} is a second messenger for these effects (1, 8).

The vacuolation response is similarly Ca^{++}-dependent. Schramm and Selinger (1) have shown that, in Ca^{++}-deficient media, secretagogues do not induce vacuole formation and that the Ca^{++}-ionophore A23187 can mimic the effects of receptor activation in bringing about vacuole formation. Thus, it has been suggested that it is the receptor-induced Ca^{++} influx that brings about vacuolation. However, Ca^{++} influx also causes K^+ efflux, Na^+ influx, and activation of the Na^+, K^+-pump (8). Therefore, these monovalent ion movements might also mediate or contribute to the vacuolation response. As discussed later, other investigators have proposed roles for Na^+ (9) and for the Na^+, K^+-pump (10) in this effect.

The purpose of this investigation was to study the vacuolation response at the light and electron microscopic levels, particularly with the aim to understand better the relationship between these various ionic fluxes and morphological changes in the cell. The results indicate a singular importance for Ca^{++} ions in vacuole formation and in morphological changes in nuclei and mitochondria as well. Monovalent ion levels do not appear to directly mediate these responses. Preliminary results of this research have appeared earlier (11, 12).

THE JOURNAL OF CELL BIOLOGY · VOLUME 97 OCTOBER 1983 1119-1130

MATERIALS AND METHODS

All experiments were performed with parotid glands removed from anesthetized (Na^+ pentobarbital, 50 mg/kg, i.p.) male Sprague-Dawley rats (90–170 g average). Glands were removed by blunt dissection and divided approximately in half with a Stadie-Riggs microtome (slice thickness ~0.5 mm, A. H. Thomas, Philadelphia, PA). Each slice was again divided in half with dissecting scissors and immediately placed in a side arm flask containing 10 ml of physiological salt solution (Krebs-Ringer-Tris, KRT[1]) of the following composition (mM): NaCl, 120.0; KCl, 5.0; $CaCl_2$, 3.0; $MgCl_2$, 1.2; β-hydroxybutyrate Na, 5.0; Tris-(hydroxymethyl)-aminomethane, 20.0, and buffered with HCl to a pH of 7.4 at 37°C. In some experiments, 0.5% BSA was added to the KRT. The flask was placed in a shaking water-bath kept at 37°C, and the KRT was continuously gassed with 100% O_2 through the side arm. All experiments were begun after a preincubation period of 25–30 min.

For study of the time course of vacuole formation, tissue pieces were then removed to either of two flasks of KRT under the same conditions for 5 min. A sample was removed from the first flask and 10^{-5} M carbachol was added to the second. Tissue was removed at intervals up to 30 min from the second flask. A second piece of tissue was removed from the first flask at 30 min.

The effect of Ca^{++} concentration on vacuole formation was investigated by incubating tissue in one of four KRT solutions containing: (*a*) no $CaCl_2$ plus 10^{-4} M EGTA; (*b*) 1 mM $CaCl_2$; (*c*) 3 mM $CaCl_2$; (*d*) 10 mM $CaCl_2$. Tissue was removed after 5 min. 10^{-5} M carbachol was then added to each flask and tissue was removed again after 10 min.

Both the reversibility of the vacuolation process and its Ca^{++}-dependence were determined by first incubating in a KRT containing no $CaCl_2$ plus 10^{-4} M EGTA. Carbachol (10^{-5} M) was added after 5 min and then 3 mM $CaCl_2$ was added 5 min later. Either atropine (10^{-6} M) or 5 mM EGTA or both were added 5 or 10 min after the addition of $CaCl_2$. Tissue samples were removed at designated intervals.

The possible roles of various ions in the vacuolation process were studied by varying external concentrations or applying blockers during stimulation. After the standard preincubation period, tissue slices were transferred to one of several flasks containing KRT with the following changes: (*a*) no change (control); (*b*) 75 mM NaCl plus 45 mM potassium isethionate (50 mM total K^+–high K^+ medium); (*c*) 30 mM NaCl plus 90 mM LiCl (35 mM total Na^+–low Na^+ medium); (*d*) no added $CaCl_2$ plus 10^{-4} M EGTA (0 Ca^{++} medium); (*e*) 10^{-3} M ouabain; (*f*) 10 mM sodium cyanide plus 1 mM iodoacetic acid. Samples were incubated in one of these oxygenated media for 10 min. Carbachol (10^{-5} M) was then added to each flask and tissue was removed after an additional 10 min. Amylase determinations were done according to Bernfield (13).

Tissue intended for morphological analyses was dropped immediately into a room temperature fixative of 2% glutaraldehyde, 2% formaldehyde (from paraformaldehyde) in 0.1 M sodium cacodylate buffer plus 1.7 mM $MgCl_2$, pH 7.4 (~650 mOsM). (10^{-4} M EGTA was added to the primary fixative in some experiments.) At the end of each experiment, the accumulated pieces were carefully minced under a magnifying light so as to preserve undamaged acini. These minced pieces, ~1mm diam, were placed in fresh fixative for a total of 2 h. The samples were washed for 30 min in room temperature buffer (0.1 M sodium cacodylate plus 3.5% sucrose, pH 7.4, ~280 mOsM) and postfixed in 1% osmium tetroxide in the same buffer for 1.5 h, also at room temperature. The samples were washed once and stored overnight in buffer at 4°C. The next morning, the samples were brought to room temperature in buffer, en bloc stained for one h in 2% aqueous uranyl acetate, dehydrated in a graded series of ethanols and propylene oxide, and embedded in Spurr's resin (14). Tissues from some experiments were infiltrated according to the rapid centrifugation method of Millonig (15).

For each experiment, three untrimmed blocks from every time point or situation were randomly chosen and 0.5-μm sections were prepared with glass knives on an ultramicrotome. These sections were mounted on glass slides and stained with 1% toluidine blue in 1% sodium borate. Each of the resulting slides was photographed through a #11 green filter and a × 16 objective lens of a Zeiss Photomicroscope and printed to a final enlargement of × 460. These micrographs were then analyzed with a Zeiss MOP-3 semiautomatic image analyzer. The fraction of cellular volume attributed to vacuoles (expressed as a percentage) was estimated as the ratio of vacuole area to the total acinar cell area measured (16, 17). Only acinar cells were measured; those cells obviously damaged or dead, i.e., with pycnotic nuclei, were eliminated. Vacuoles smaller than 2-μm in diam (1 mm on the print) were not measured. Measurements from the three micrographs (slides) for each experimental condition were pooled to obtain one value for the percent volume density of vacuoles. Experiments were carried out at least three times; means and standard errors were calculated. Statistical significance was determined by one- or two-way analysis of variance. The critical probability for rejection of the null hypotheses was 5% throughout.

One tissue block from each experiment which gave a percent volume density value close to the mean for that experimental condition was trimmed and thin-sectioned with a diamond knife. Silver sections were retrieved on copper grids, stained either for 1 min with 0.2% lead citrate (18) or for 2 min in saturated uranyl acetate in 50% ethanol and 1 min in lead. The grids were viewed in either a Hitachi HU-12 or a Philips EM 400 electron microscope at an accelerating voltage of 50 or 60 kV, respectively. Six micrographs were taken of sections from each of these blocks at a magnification of × 3,500–3,600 and printed to a total enlargement of × 7,000. Experiments were done at least three times which gave a total of 18 micrographs for each situation. These micrographs were then subjectively evaluated for changes in the following: nuclear shape and chromatin distribution, mitochondrial conformation and presence or absence of intramitochondrial granules, appearance of the Golgi complex, and the presence of an obvious abundance of small, smooth-membrane vesicles in the cytoplasm.

RESULTS

Characterization of the Vacuolation Response

Light Microscopy and Morphometric Analyses: Parotid tissue slices incubated in normal KRT for 1 h (30-min preincubation plus 30 min additional) retained the appearance of normal tissue processed immediately upon removal from the rat (Fig. 1 *a*). Normal acinar cell polarity was maintained, along with normal cell-cell contacts within acini. We have shown in previous studies that these slices are stable with respect to oxygen consumption, water content, cation content and ultrastructure for up to 2 h of total incubation time (19). All of the experiments in this study were done within this time-frame.

When 10^{-5} M carbachol was added to the normal incubation medium, large cytoplasmic vacuoles appeared within 5 to 10 min as observed in the light microscope (Fig. 1 *b*). Some exocytosis was apparent (19), but the most obvious change in cellular appearance at the light microscope level was the presence of clear vacuoles ranging in size from 1 to 20 μm in diameter. Acinar cells appeared normal in other respects.

This receptor-mediated vacuolation response was dependent on extracellular Ca^{++}. The response was quantitated (as described in Materials and Methods) as the change in the percent volume density of vacuoles as shown in Fig. 2. Tissue slices incubated in KRT solution with no added $CaCl_2$ plus 10^{-4} M EGTA and with 10^{-5} M carbachol did not vacuolate until excess $CaCl_2$ was added; the response was then immediate. To determine the concentration of extracellular Ca^{++} for an optimal response, tissue slices were incubated in KRT solutions with differing amounts of $CaCl_2$ for 10 min. Significant vacuolation responses were obtained when carbachol was added with 3 mM and 10 mM $CaCl_2$ concentrations (Table I); however, carbachol in the presence of 10 mM $CaCl_2$ also caused a substantial increase in the number of disrupted cells and cells with pycnotic nuclei. 3 mM $CaCl_2$ was therefore used throughout the study. Increasing the extracellular Ca^{++} concentration in the absence of an agonist did not induce substantial vacuole formation (Table 1). Conversely, carbachol added to media containing no Ca^{++} had little effect (Table 1).

The extent of vacuolation was time-dependent (Fig. 3). When carbachol was added to normal incubation medium (containing 3 mM $CaCl_2$), the percent volume density of vacuoles increased from control values below 0.5% to 3% in 10 min and finally to over 7% in 30 min. The response did not appear to reach a maximum within 30 min, in contrast to results by Schmidt et al. (2) who reported that dispersed parotid acini appear to respond maximally (11% V_v) within 5 min after the addition of carbachol. This difference may be

[1] *Abbreviations used in this paper:* KRT, Krebs-Ringer-Tris; $\%V_v$, percent volume density of vacuoles.

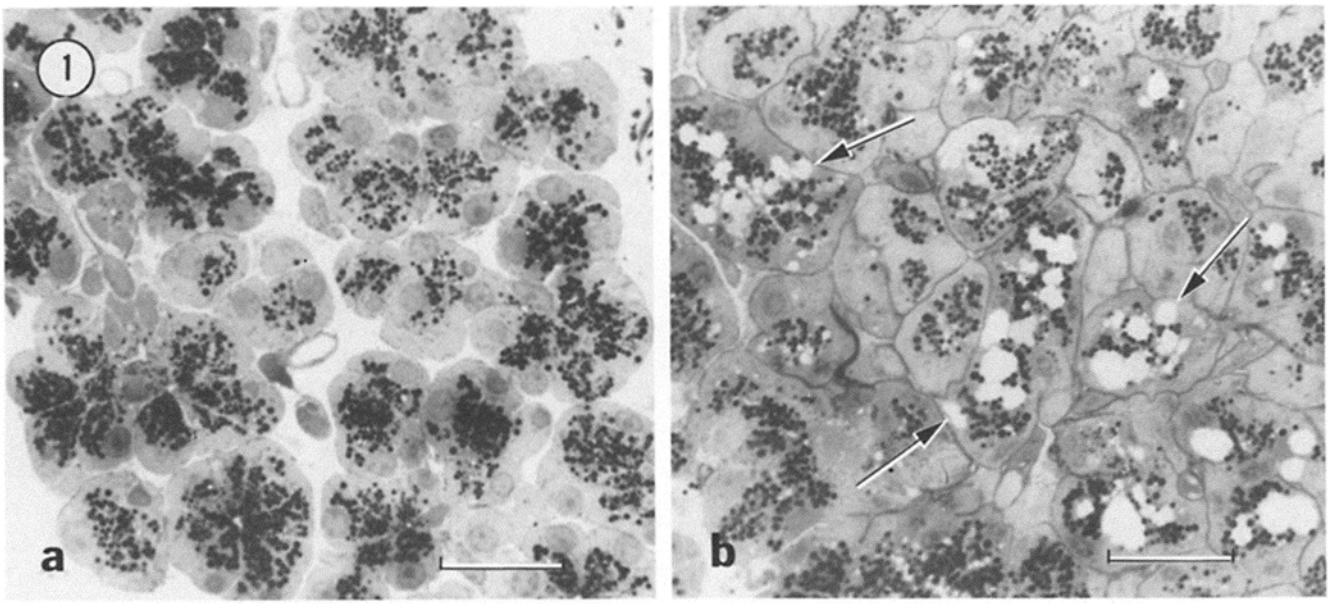

FIGURE 1 Light micrographs of incubated parotid tissue. (a) Control tissue incubated for 30 min in KRT containing 3 mM $CaCl_2$. Note retention of normal acinar structure and maintenance of cellular polarity within the slice. (*b*) Tissue incubated in same buffer plus 10^{-5} M carbachol for 10 min. Large, clear vacuoles have appeared throughout the tissue (arrows). The tissue otherwise appears normal. Bar, 20 μm. × 800.

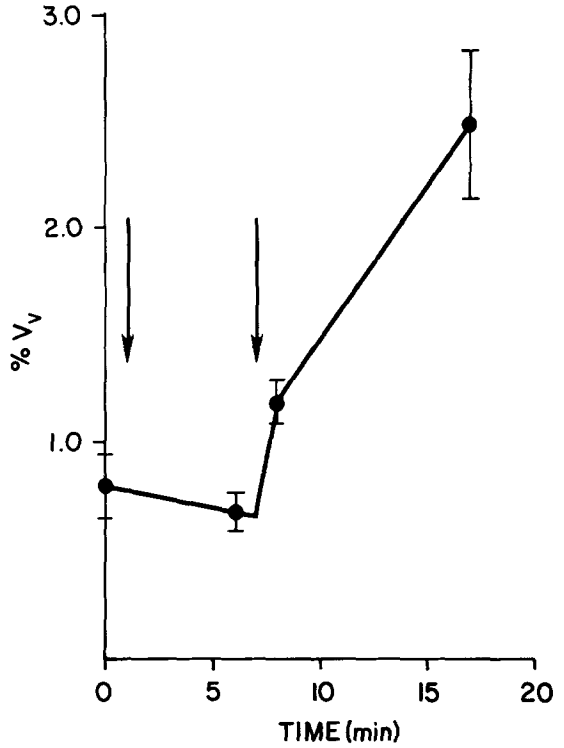

FIGURE 2 Calcium ions must be present for carbachol-induced vacuoles to appear. This graph shows the time course of the change in percent volume fraction of vacuoles in slices stimulated with carbachol and Ca^{++}. After 30-min preincubation, tissue slices were incubated for 5 min in KRT with no added Ca^{++} plus 10^{-4} EGTA. 10^{-5} M carbachol was added at the first arrow and 3 mM $CaCl_2$ was added at the second. Means ± SEM, $n = 8$.

due to differences in stability of slice preparations vs. dispersed acini. Basal levels of percent volume density of vacuoles reported by Schmidt and co-workers (2) are much higher than the values obtained in this study (3.5% vs. ~0.6%, respectively).

TABLE 1

Effect of Ca^{++} Concentration on Carbachol-induced Vacuoles

[Ca^{++}]	− Carbachol (10 min)	+ Carbachol (10 min)
mM	% V_v	% V_v
0	0.90 ± 0.20 (4)	0.53 ± 0.07 (3)
1	0.26 (1)	1.19 ± 0.28 (3)
3	0.65 ± 0.08 (10)	2.93* ± 0.37 (16)
10	0.91 (1)	3.99* ± 1.01 (3)

Means ± SEM. Numbers in parentheses are the number of animals.
* Statistically significant.

Electron Microscopy: Tissue slices incubated in KRT with no added $CaCl_2$ plus 10^{-4} M EGTA and with 10^{-5} M carbachol appeared identical to tissue incubated in either the same medium without carbachol or in normal KRT (Fig. 4*a*). The generally polarized nature of the acinar cell evident in the light microscope was still obvious. Nuclei were rounded with peripherally-distributed heterochromatin, and slightly less electron-dense nucleoli. Both extensive arrays of rough endoplasmic reticulum and well-defined Golgi regions were prominent. Mitochondria were condensed with electron-dense matrices and contained several electron-dense granules. The numerous secretory granules were variable in electron density. These observations agreed with previously published studies on the rat parotid (20). Small, smooth-membrane vesicles (100–120-nm diam) were occasionally seen directly beneath the basal and lateral plasma membrane.

Once stimulated (by adding either Ca^{++} to carbachol-containing medium or carbachol to Ca^{++}-containing medium), this appearance changed dramatically. As also seen in the light microscope, the most obvious change was again the development of cytoplasmic vacuoles near the Golgi region, the area between the nucleus and the secretory granules (Fig. 4, *b* and *c*). With time, these vacuoles increased in number and size until, in some cases, they occupied most of the cell volume. It was difficult to determine the location of the origin of these very large vacuoles. However, even in cells containing

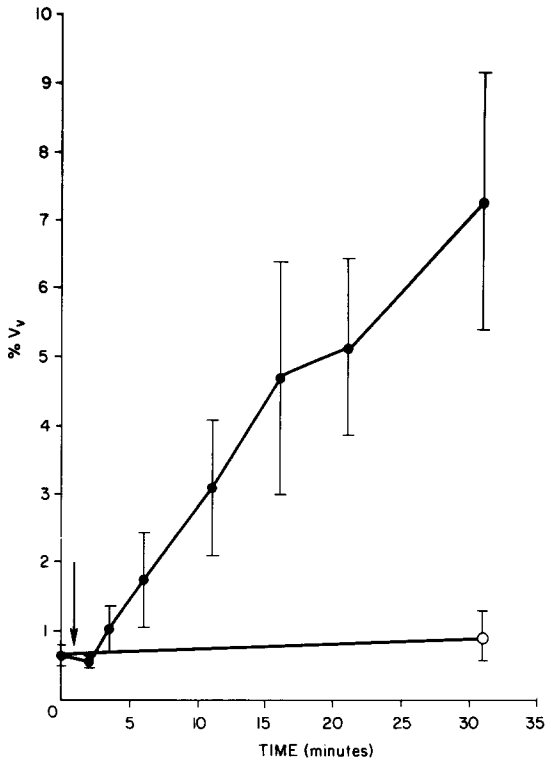

FIGURE 3 Time course of carbachol-induced vacuole formation. After preincubation, tissue slices were placed in KRT containing 3 mM $CaCl_2$. For the closed circles (●), 10^{-5} M carbachol was added at the arrow. The open circle (○) represents tissue incubated in the same buffer without carbachol for the duration of the experiment. Means ± SEM; $n = 3$–7.

large vacuoles (>10 μm), smooth-membrane cisternae of the Golgi complex often were seen lying in close apposition to the vacuole (Fig. 4, *inset*). Because of this observation, we suspect that the condensing vacuole or immature granule may be the source of these vacuoles and not the Golgi cisternae proper. We have no other data to support this contention, however. At later stages, secretory granules can be seen fusing with the vacuole membrane and emptying their contents into the vacuole space (not shown). Vacuoles often contained flocculent material, isolated pieces of membrane and, occasionally, myelin figures.

Enlarged lumens, with scalloped borders reminiscent of secretory granules (19) often were more obvious at earlier times than later, presumably because of the obscuring effects of the large vacuoles. The secretory rate of α-amylase has been shown to remain relatively constant for as long as 40 min with continuous stimulation (21).

Concomitant with vacuole formation, other ultrastructural changes were observed. The nuclei became misshapen; the heterochromatin was condensed and the nucleoli became more prominent (Fig. 5, *a* and *b*). The mitochondria swelled somewhat, resulting in electron-lucent matrices and parallel-sided cristae (Fig. 5, *c* and *d*). Both nuclear and mitochondrial changes were evident 1 min after carbachol was added, much sooner than vacuole development (Fig. 3). Intramitochondrial granules, however, disappeared between 5 and 10 min of carbachol stimulation. At later stages, i.e., 30 min (Fig. 4*c*), an increase in the size and number of smooth-membrane vesicles was observed throughout the cell. Golgi cisternae were swollen, and smooth-membrane vesicles located under the basal and lateral plasmalemma were enlarged. Mitochondria swelled considerably and lost cristae. In some cases, the cisternae of the rough endoplasmic reticulum were slightly swollen and contained a material of medium electron density, as did the spaces between the nuclear and rough endoplasmic reticulum membranes.

Reversal of the Vacuolation Response

Light Microscopy and Morphometric Analyses: If this vacuole response is truly a receptor-mediated event, it should be blocked or inhibited by a specific receptor-blocking drug. Since this response is presumably Ca^{++}-mediated, it should also be blocked by the removal of extracellular Ca^{++} once stimulated. When either 10^{-6} M atropine, a muscarinic-cholinergic antagonist, was added or extracellular Ca^{++} was removed with an excess amount (5 mM) of EGTA, the vacuolation response to carbachol, as measured from the light micrographs, was reversed. When these agents were added 5 min after Ca^{++} was added to carbachol-containing medium, the reversal was immediate (in the time-frame of these experiments; Figs. 6 and 7). The values obtained 15 min after either atropine or EGTA was added were significantly reduced from values for the normal response at equivalent times and were similar to control values. When these same agents were added (singly or together) 10 min after stimulation, the reduction in vacuolation was not so immediate (Fig. 8). However, after 15 min the values obtained were significantly reduced from the normal response. Additional samples to which EGTA had been added were removed after 30 min (not shown), and in these cases values for percent volume density of vacuoles averaged 1.88 ± 0.08 ($n = 3$). The normal vacuolation response to carbachol (7.27 ± 1.88 at 30 min, Fig. 3) was arrested under these conditions.

Electron microscopy: As indicated in Fig. 8, some vacuoles, although reduced in size and number, were still present. However, the other ultrastructural changes occurring with carbachol stimulation were completely reversed when the vacuolation response was either completely blocked (Fig. 6) or inhibited (Fig. 8). The time course of the restoration of normal structure appeared to vary somewhat depending on

FIGURE 4 Electron micrographs of vacuole formation in parotid tissue. (a) Tissue incubated for 10 min in KRT containing 3 mM $CaCl_2$ displays normal cellular architecture: heterochromatin is fibrillar, mitochondria (*m*) are condensed with granules, Golgi apparatus (*G*) and condensing vacuoles are apparent. (*b*) Tissue incubated in the same medium plus 10^{-5} M carbachol for 10 min shows typical morphological changes: vacuoles (*V*) prevalent in the Golgi area, markedly condensed heterochromatin, swollen mitochondria (*m*) with few if any granules. (*c*) At 30-min stimulation with carbachol, the effect is much more dramatic. Vacuoles now occupy much of the volume of the cell and contain membranous debris. Evidence of exocytosis into the lumen (*L*) is prominent. Nuclei are misshapen, and the remaining Golgi apparatus is swollen as is some of the rough endoplasmic reticulum (*rer*). (*Inset*) The entire Golgi apparatus does not participate in vacuole formation. Bracket indicates part of the Golgi system lying near a vacuole. Bars, 1 μm. × 6,100 (*a*); × 6,800 (*b*); × 7,500 (*c*); × 23,000 (*inset*).

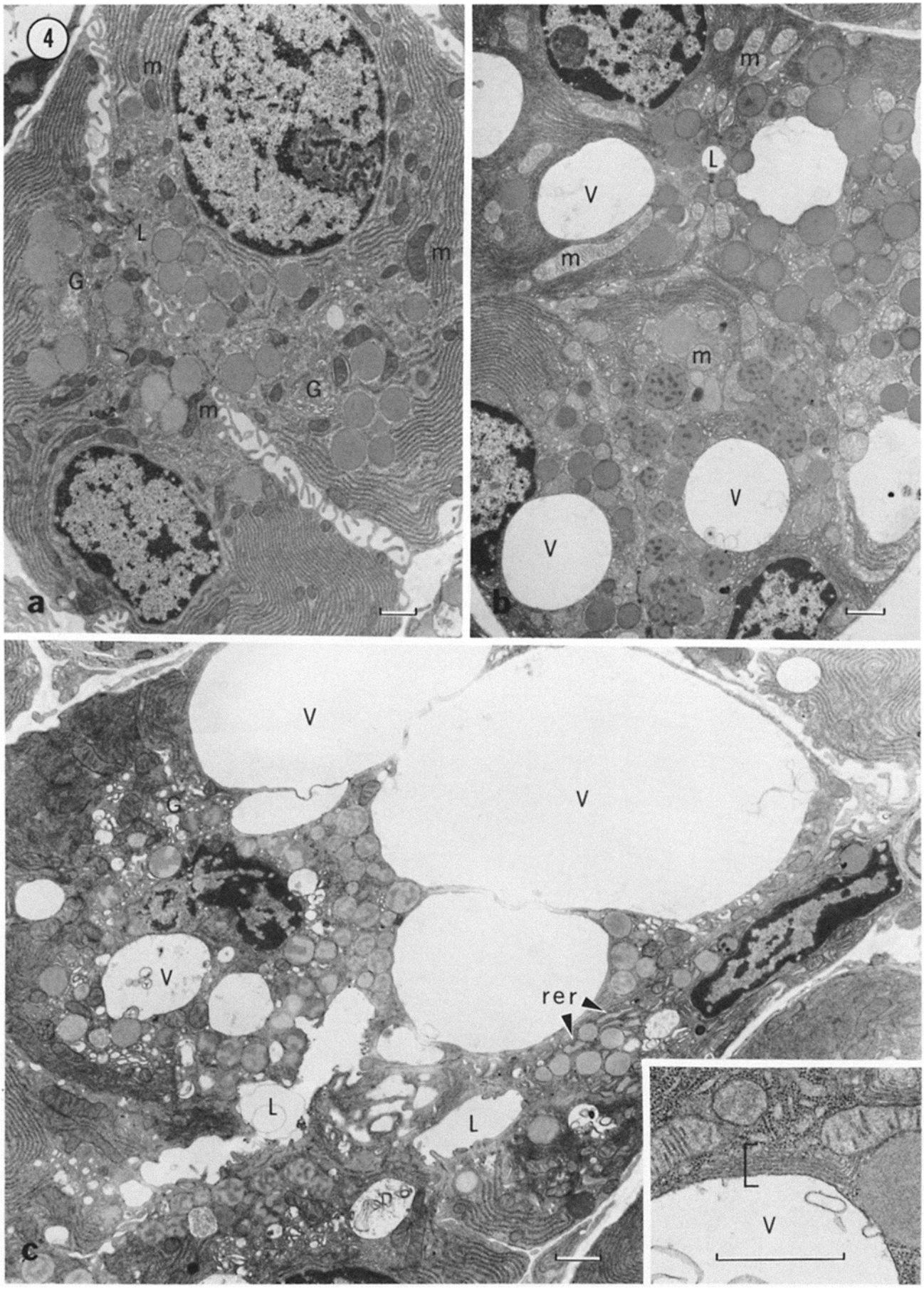
4
m
L
G
m
G
m
a
m
L
V
m
m
V
V
b
V
V
G
V
rer
L
L
n
c
L
V

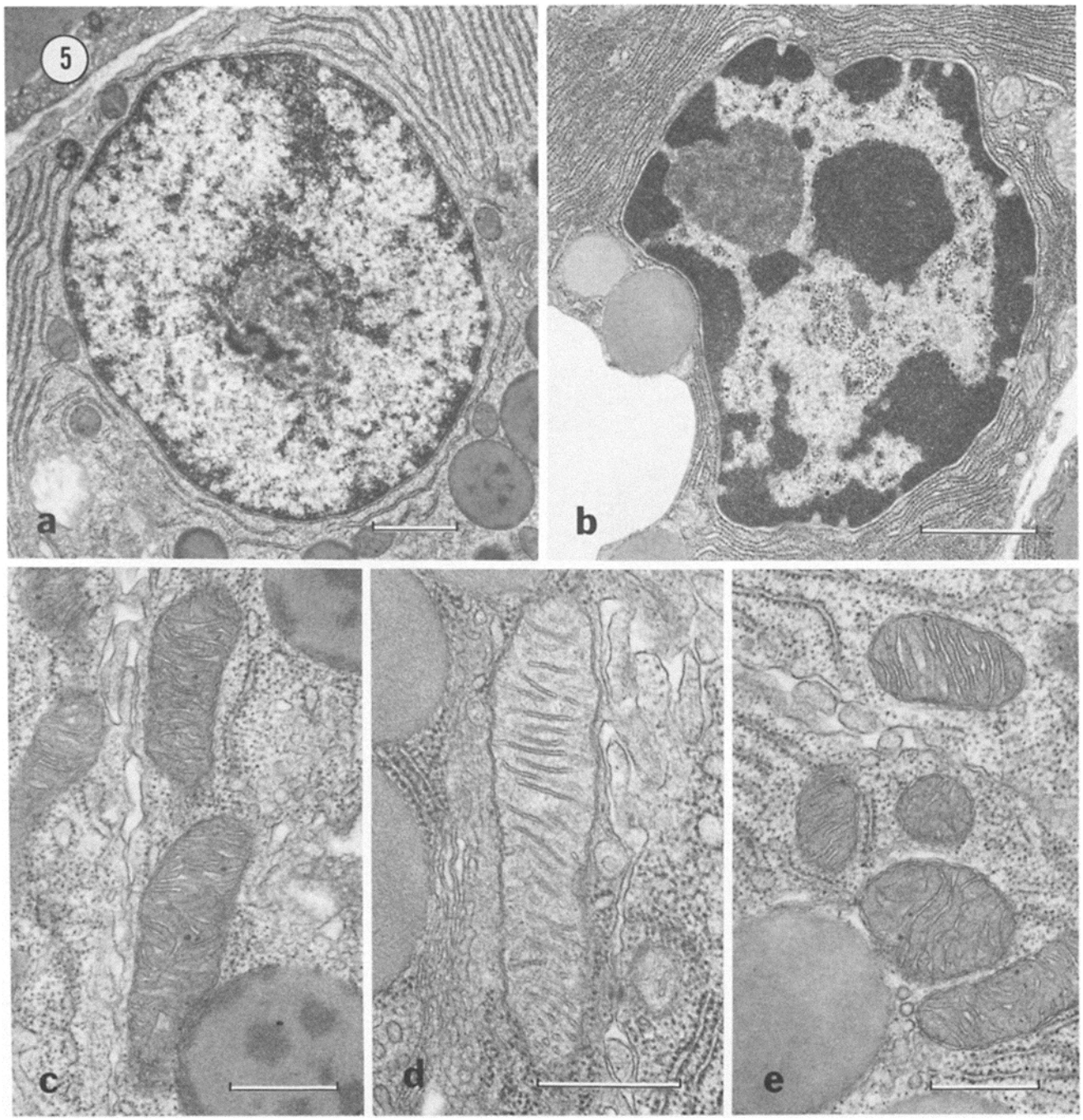

FIGURE 5 The effects of carbachol are qualitatively the same whether the drug is added to Ca^{++}-containing media or Ca^{++} is added to carbachol-containing media. These micrographs are all from the same experiment. (*a*) Nucleus from tissue incubated for 5 min in KRT with no Ca^{++} plus 10^{-5} M carbachol. (*b*) The change in nuclear configuration is apparent upon the subsequent incubation in 3 mM $CaCl_2$ for 10 min. (*c–e*) Changes in mitochondrial conformations. (*c*) Tissue incubated as in *a* showing condensed mitochondria with granules. (*d*) Swollen mitochondria after the addition of 3 mM $CaCl_2$ as in *b*. (*e*) Mitochondrial conformations are reversible upon the removal of Ca^{++} with the subsequent addition of 5 mM EGTA for 30 min. (*a* and *b*) Bars, 1 μm. × 13,000 (*a*); × 18,000 (*b*). (*c–e*) Bars, 0.5 μm. × 35,000 (*c*); × 45,000 (*d*); × 35,000 (*e*).

the subcellular organelle involved. In general, the ultrastructural appearance of mitochondria and nuclei returned to normal almost immediately, whereas the loss of cellular vacuoles was more gradual. Fig. 9 shows that cells that still contained a few small vacuoles and swollen Golgi have mitochondria and nuclei that have returned to control appearances. The ultrastructural effects of reversing vacuole formation with EGTA when compared with atropine did not reveal any qualitative differences (see also Fig. 5*e*). The addition of carbachol to media containing atropine in the presence of Ca^{++} had no effects on parotid ultrastructure (2, 19).

Effects of Ion Substitutions and Metabolic Inhibitors on Vacuole Formation

It has been shown that carbachol increases Ca^{++} permeability of the plasmalemma of parotid cells (22, 23) and that

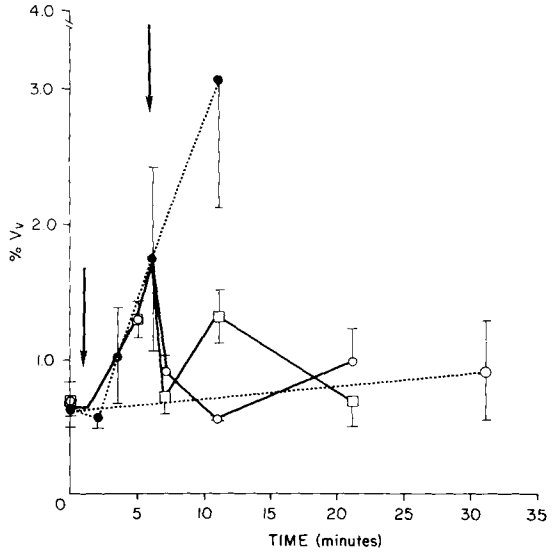

FIGURE 6 Reversal of vacuole formation. Tissue was incubated (after a 30-min preincubation) in KRT with no added Ca^{++} plus 10^{-4} M EGTA and 10^{-5} M carbachol. 3 mM $CaCl_2$ was added at the first arrow. 5 min later at the second arrow, either 5 mM EGTA (○) or 10^{-6} M atropine (□) was added. The normal time course of vacuole formation (Fig. 3) has been superimposed in dotted lines for comparison. (n = 3).

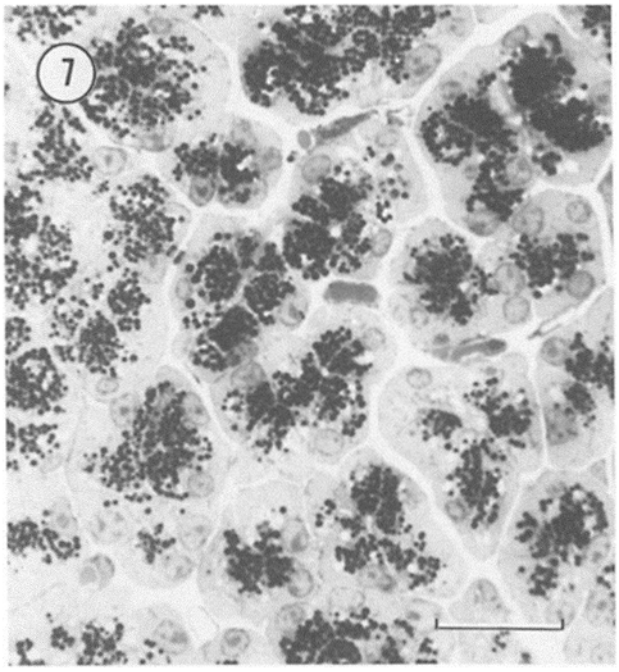

FIGURE 7 Reversal of vacuole formation. Light micrograph of parotid tissue incubated for 15 min in 10^{-6} M atropine subsequent to a 5-min incubation in calcium-containing buffer plus carbachol, a representative sample from the experiments in Fig. 6. Vacuoles have been reduced considerably. Bar, 20 μm. × 800.

the resulting increase in internal Ca^{++} triggers substantial K^+ efflux and Na^+ influx occurring with carbachol stimulation (8, 24). To determine whether the secondary Na^+ or K^+ movements due to carbachol are involved in vacuole formation, ion substitution regimens were used to either reduce (low Na^+ and high K^+ media) or exacerbate (ouabain) these fluxes.

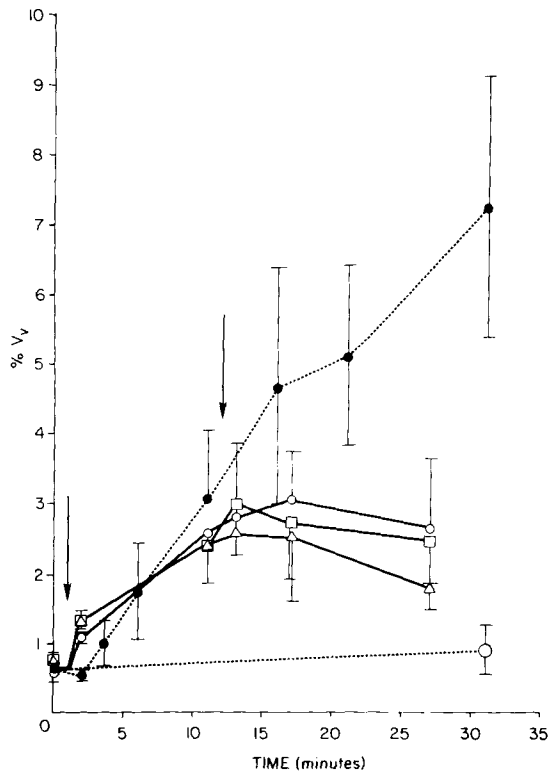

FIGURE 8 Inhibition of vacuole formation. As in Fig. 6, tissue was incubated for 5 min in KRT with no added Ca^{++} plus 10^{-4} M EGTA and 10^{-5} M carbachol. 3 mM $CaCl_2$ was added at the first arrow. 10 min later at the second arrow, either 5 mM EGTA (○), 10^{-6} M atropine (□), or both (△) were added. As in Fig. 6, Fig. 3 has been superimposed for comparison. (n = 3–4).

Light Microscopy and Morphometric Analyses: Incubation of parotid tissue slices in KRT solutions with no Ca^{++}, with high K^+ concentration (50 mM vs. 5 mM) or with low Na^+ concentration (35 mM vs. 125 mM) had little effect on vacuole formation over control levels (Fig. 10). However, when carbachol was added for an additional 10 min, differences could be seen. Both the high potassium medium and the Ca^{++}-free medium significantly inhibited carbachol-induced vacuole formation. However, lowering the Na^+ concentration of the incubation medium had little effect on the increase in percent volume density of vacuoles due to carbachol.

Despite the fact that the values for percent volume density of vacuoles were similar for both the absence of Ca^{++} and the high $[K^+]$ incubations, the appearance of the respective tissues in the light microscope was very different. Incubation in KRT with high potassium concentrations with or without carbachol caused extensive degranulation, resulting in enlarged lumens. Additional experiments (n = 4) were carried out to measure α-amylase secretion under these conditions. Incubation in KRT containing 50 mM K^+ caused 2.26 ± 0.55% amylase to be secreted in 30 min compared with a control secretion rate of 0.36 ± 0.17%. The secretion due to high K^+ has been shown to be due to the release of catecholamines from endogenous nerve endings (25). In normal medium, carbachol caused a 0.95 ± 0.57% secretion rate. In high K^+ medium, however, carbachol did not stimulate amylase secretion if propranolol was present to block the effects of released catecholamines (0.44 ± 0.16%).

Ouabain alone had little effect on vacuole formation but

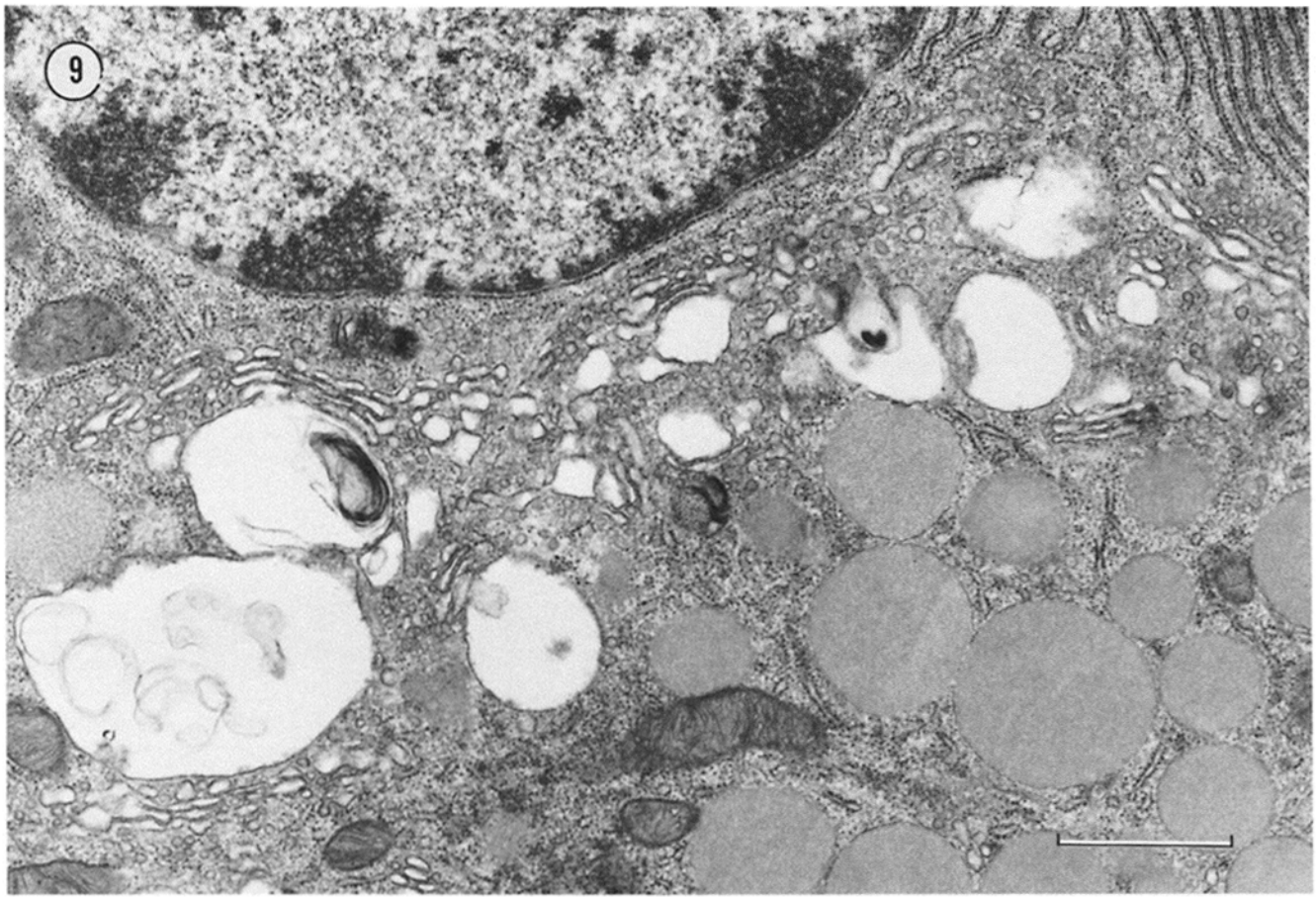

FIGURE 9 Electron micrograph of vacuole inhibition. Slices were incubated in medium containing 3 mM $CaCl_2$ and 10^{-5} M carbachol for 10 min, at which time 10^{-6} M atropine was added to the medium. Incubations were continued for an additional 15 min, at which time tissues were removed and fixed. Some swelling is still present in the Golgi apparatus; however, nuclei and mitochondria have returned to the configurations present in control tissue. Bar, 1 μm. × 22,000.

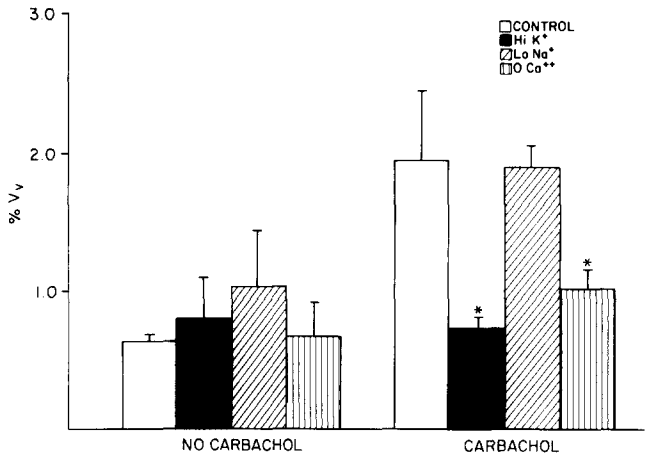

FIGURE 10 Effects of altered extracellular cation concentrations on vacuole formation. Tissue slices, after preincubation, were incubated for 10 min in one of the following buffers (see Materials and Methods for complete compositions): *control*, KRT containing 3 mM $CaCl_2$; *Hi* K^+, KRT containing 50 mM K^+ instead of 5 mM; *Lo* Na^+, KRT containing 35 mM Na^+ instead of 125 mM; and *0* Ca^{++}, KRT with no $CaCl_2$ plus 10^{-4} M EGTA. Samples were removed and then 10^{-5} M carbachol was added to each buffer for an additional 10 min. The final samples were then removed and processed as described. (*, statistically significant differences from control; n = 3).

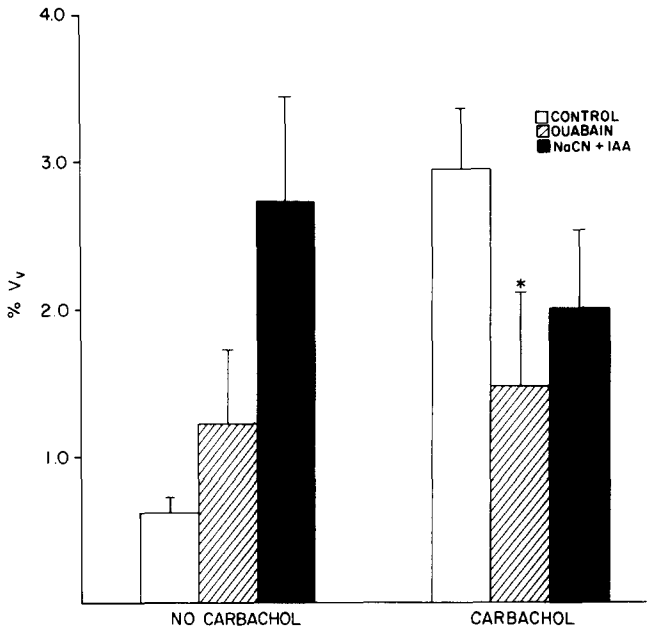

FIGURE 11 Effects of metabolic inhibitors. Protocol was similar to that of Fig. 10, except: *ouabain*, KRT plus 10^{-3} M ouabain; *NaCN + IAA*, KRT plus 10 mM cyanide and 1 mM iodoacetic acid. Incubations were carried out for two 10-min periods; carbachol was present during the second period. (*, statistically significant differences from control; n = 6).

significantly inhibited the response to carbachol (Fig. 11). The metabolic inhibitors cyanide and iodoacetic acid caused parotid acinar cells to vacuolate; this response was not further increased by addition of carbachol.

Electron Microscopy: In agreement with results obtained with the light microscope, the electron microscope revealed evidence for extensive exocytosis in tissue incubated in high K^+ concentrations whether carbachol was present or not. Incubation without carbachol in the other buffers (normal KRT, high Na^+, no Ca^{++}; not shown) yielded essentially the same ultrastructural appearance, i.e., similar to control tissues. Fig. 12*a* is an example of parotid tissue incubated for 10 min in KRT with 50 mM K^+ followed by 10 min with an addition of 10^{-5} M carbachol. Active secretion was obvious from the enlarged lumens but the structural changes associated with carbachol stimulation were not apparent. Large vacuoles were not present, confirming the light microscope data. Heterochromatin of the nuclei was similar to that of control cells, i.e., not markedly condensed, and the mitochondria were condensed with occasional electron-dense granules. Golgi cisternae were not obviously swollen and contained condensing vacuoles similar to those found in the control tissue. Incubations in buffer with no Ca^{++} plus carbachol yielded an appearance similar to that of control tissues, i.e., no vacuoles or exocytosis, and incubation in normal KRT plus carbachol yielded the changes associated with carbachol as described earlier. Morphological effects of carbachol in low Na^+ KRT (Fig. 12*b*) were similar to those obtained in normal media. Fig. 12*b* reveals misshapen nuclei with condensed heterochromatin, swollen mitochondria with few, if any, granules, and large vacuoles associated with the Golgi complex.

Ouabain alone did little to change the ultrastructural appearance of these cells (Fig. 13*a*). Some cells exhibited swollen Golgi and a few small vacuoles as evidenced by the slightly higher values for percent volume density of vacuoles over control (Fig. 11). Ouabain, however, inhibited not only large vacuole formation but also the other ultrastructural changes caused by carbachol (Fig. 13*b*). Nuclear chromatin retained its normal appearance as did the mitochondria. Retention of intramitochondrial granules was extremely variable, however.

Metabolic inhibitors (Fig. 13, *c* and *d*), on the other hand, had a more deleterious effect on cellular ultrastructure. As seen in Figs. 11 and 13, *c* and *d*, no qualitative or quantitative differences could be determined with or without carbachol. Large vacuoles were present under both conditions. Nuclear heterochromatin was markedly condensed and the nucleoli were very obvious. Mitochondria lost their granules and were swollen, in some cases to the point of disruption.

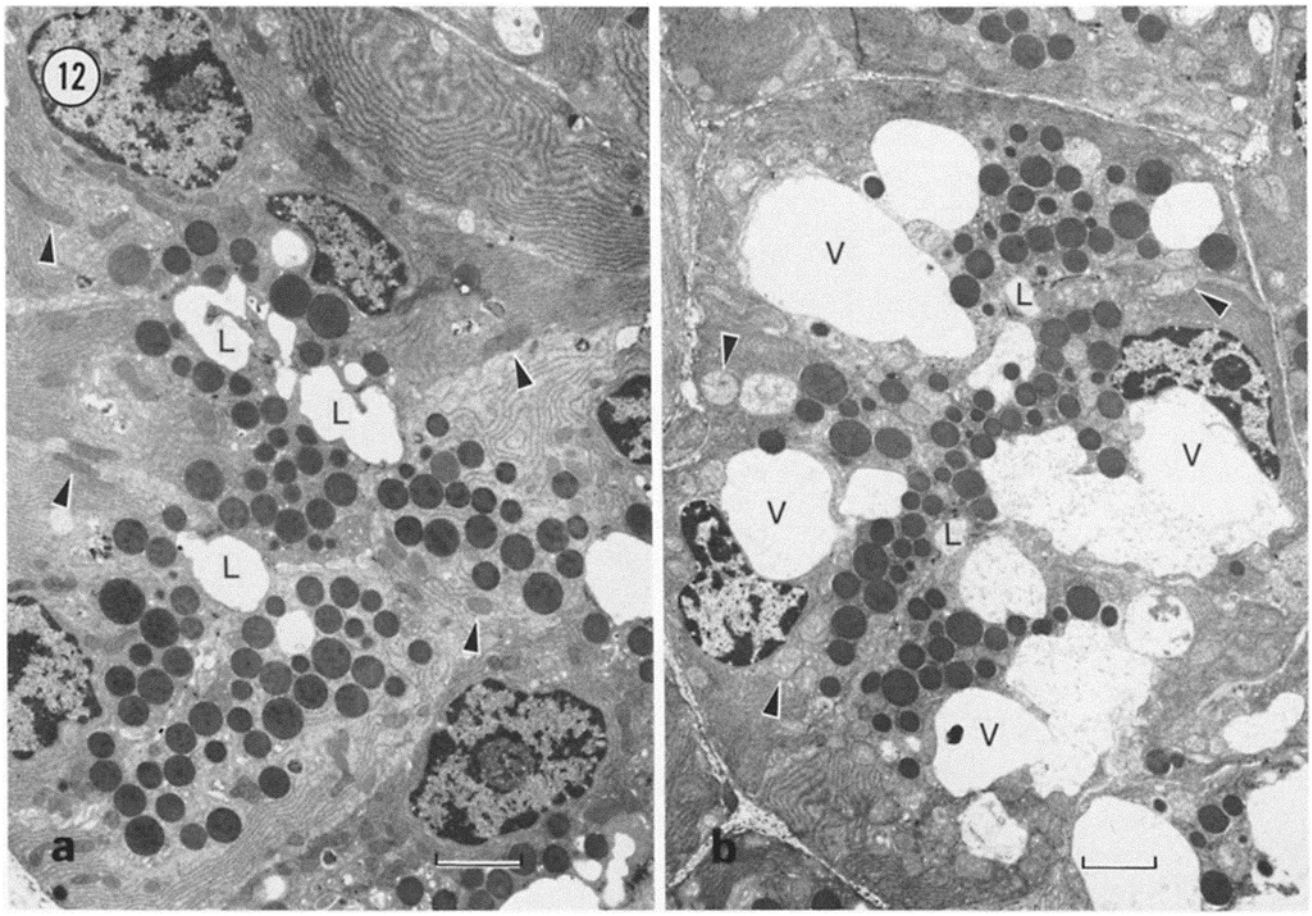

FIGURE 12 Parotid tissue stimulated with carbachol in the presence of either high K^+ concentrations (a) or low Na^+ concentrations (*b*). These are representative samples from experiments graphed in Fig. 10. (a) Agonist-induced vacuole formation is completely blocked by 50 mM K^+. However, enlarged lumens (*L*) are evidence of increased amylase secretion, presumably due to depolarization-induced catecholamine release. Nuclear heterochromatin is fibrillar and mitochondria (arrowheads) are condensed and contain occasional intramitochondrial granules. (*b*) Carbachol-induced vacuole formation (*V*) is unaffected by 35 mM Na^+. Heterochromatin is markedly condensed and mitochondria are swollen. Bars, 2 μm. × 5,200 (a); × 4,600 (*b*).

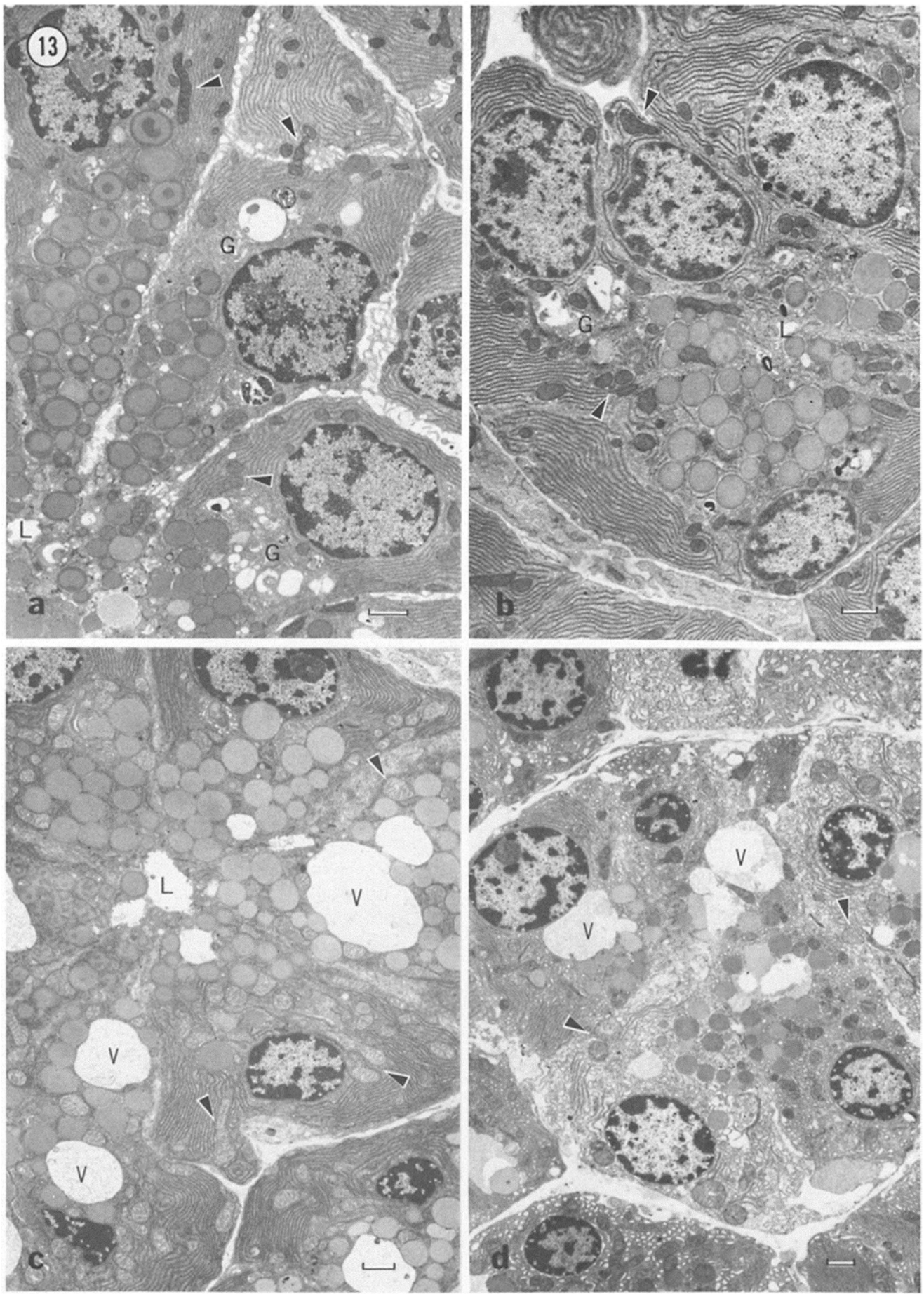
13
G
L
G
a
G
L
b
L
V
V
V
c
V
V
d

DISCUSSION

With cholinergic stimulation, rat parotid cells take up Ca^{++} and secondarily gain Na^+ and lose K^+ (8). Thus any one of these ionic events could play a role in the stimulation-induced vacuolation response. The results of this study, however, indicate that Ca^{++} influx is likely the primary stimulus for vacuole formation, rather than movements of the monovalent ions. The evidence can be summarized as follows.

The vacuolation process could be initiated by the addition of Ca^{++} to carbachol containing medium and could be reversed or significantly inhibited by the removal of Ca^{++} (Figs. 2, 6, and 8). Previous studies have shown that Ca^{++} ionophores can mimic the effects of receptor activation in inducing vacuoles (1, 26). These results confirmed earlier findings and indicated that an elevation in cytosolic Ca^{++} can induce vacuole formation; however, since Ca^{++} causes substantial Na^+ gain and K^+ loss (8), it is not clear whether Ca^{++} directly mediates the response or whether the Na^+ or K^+ movements are responsible. The experiments summarized in Fig. 10 showed that increasing extracellular K^+, and thereby inhibiting net K^+ loss (27), blocked agonist-induced vacuole formation. Decreasing external Na^+, which should decrease Na^+ gain (28), had no effect. Since salivary fluid secretion is apparently a sodium-dependent process (29), this argues against any relationship between fluid secretion and the morphological changes. These results then could be taken to indicate that it is the K^+ loss rather than the Na^+ gain that triggers the response. If this is so, then ouabain should exacerbate the response since it has been shown that ouabain substantially potentiates the agonist-induced net loss of K^+ by inhibiting the Na^+, K^+-ATPase (30). Precisely the opposite result was obtained, however; ouabain blocked the vacuolation response to carbachol.

Besides preventing K^+ loss, incubation of parotid cells in a high K^+ medium also substantially decreases the plasma membrane potential (31). When carbachol and ouabain are added to parotid cells, ionic gradients are almost completely dissipated (32). This would also be expected to result in plasma membrane depolarization. When electrically inexcitable cells are depolarized, carbachol-induced Ca^{++} influx is significantly inhibited (33). Consistent with this view is the finding that depolarization also inhibits carbachol-induced amylase secretion (this study and reference 34), a response believed due to Ca^{++} influx (19). Thus, it would appear that the prevention of vacuole formation by high K^+ and by ouabain may be due to membrane depolarization and subsequent inhibition of Ca^{++} influx, rather than alterations in monovalent ion shifts.

Metabolic inhibitors such as cyanide and iodoacetate also caused vacuoles to form in parotid cells with Ca^{++} and no other stimulus. When electron transport is blocked, cellular ATP levels fall and calcium gradients can no longer be maintained. The structural effects of these agents were more severe with long-term administration than with carbachol alone (Fig. 13*d*).

Nuclear condensation and mitochondrial conformational changes occurred in concert with vacuole formation and could not be dissociated from it, at least with the experiments in this study. Vacuolated cells always had condensed nuclei and orthodox or swollen mitochondria; and conversely, nonvacuolated cells had nuclei with normally dispersed chromatin and condensed mitochondria. These morphological effects were apparently not a cytotoxic response to the experimental conditions (although they do bear a striking resemblance to them as will be discussed later), as they could be reversed or inhibited by the addition of atropine. Also, Schmidt et al. (2) have shown that vacuoles stimulated to form by acetylcholine disappear after the addition of acetylcholine esterase.

The overall appearance of vacuolation, clumping of nuclear chromatin and swollen mitochondria seen in the cases of metabolic poisoning in this study, approaches the description given by Trump (9) for the early stages of cell injury. In these early stages, the changes are reversible. Over a longer period of time the changes become dramatically severe and irreversible, leading to cell death. Trump and also Farber (35) have advocated that a common occurrence in any number of cell injuries leading to death is a rise in intracellular Ca^{++} concentration, i.e., a disruption of normal Ca^{++} homeostasis.

Vacuoles formed either by cholinergic-stimulation or by cell injury have in common a dependency on extracellular Ca^{++}, although in some specific cases there is evidence for Na^+ involvement as well. Human (36) and rat fibroblasts (37) have been observed to vacuolate in the Golgi region on very long incubations (3–7 h) in monensin (an Na^+ ionophore). Smooth muscle cells from rabbit pulmonary artery do not vacuolate in the presence of cyanide and iodoacetate but do vacuolate with the rather nonspecific ionophore X537A (38). Disruption of Na^+-Ca^{++} exchange mechanisms may thus be involved in vacuolation of the Golgi in some cell types. However, this mechanism does not appear to be operating in parotid cells. Resting Ca^{++} influx is not increased by lowering external Na^+, although carbachol-induced Ca^{++} influx is slightly increased (22). Na^+-uptake by carbachol is accentuated by ouabain but vacuole formation and other morphological effects are blocked. Thus, internal Na^+ levels have little immediate effect on parotid morphology.

Vacuoles in the serous cells of the submucosal gland have been observed to occur upon α-adrenergic or cholinergic stimulation (5, 6). Because a purified preparation of serous cells from the submucosal gland is not available, there are no data on cellular ion fluxes during conditions of stimulated water flow. What has been observed is morphologically very similar to the changes described for the cholinergically-stimulated parotid gland in the present study. Both nuclear and mitochondrial changes were noted by Basbaum and co-work-

FIGURE 13 Parotid tissue incubated in either 10^{-3} M ouabain (*a* and *b*) or 10 mM sodium cyanide and 1 mM iodoacetic acid (*c* and *d*). *b* and *d* were additionally incubated in 10^{-5} M carbachol. These are representative samples from experiments graphed in Fig. 11. (*a* and *b*) Tissue incubated in ouabain plus carbachol is qualitatively similar to tissue incubated for 10 min in ouabain alone. Vacuole formation has been inhibited in this tissue as have the other carbachol-induced changes in the nuclei and mitochondria (arrowheads). Both tissues appear similar to control. (c and *d*) Tissue incubated in cyanide and iodoacetic acid, whether or not carbachol was present, shows dramatic changes. Large vacuoles (*V*) are present throughout the tissue, heterochromatin is condensed and mitochondria (arrowheads) are swollen and have lost granules. No additional vacuole formation due to carbachol was observed. *L*, lumen; *G*, Golgi complex. Bars, 1 μm. × 64,000 (*a*); × 6,300 (*b*); × 5,200 (c); × 4,300 (*d*).

ers (5) after cholinergic and α-adrenergic stimulation. The stimulated vacuoles in the serous cells were observed to arise from either condensing vacuoles or immature granules. Quinton (10) reported that vacuole formation is blocked by ouabain and suggested a model for their formation involving Na^+-influx. The results of the present study and the known relationship of ion movements in the parotid gland may indicate that depolarization and subsequent inhibition of Ca^{++} influx may explain the ouabain effect in submucosal glands as well.

The precise mechanism by which elevation of intracellular Ca^{++} causes these morphological changes cannot be deduced from these data. Some admittedly speculative possibilities that should be the subject of future investigations are suggested here. As the intracellular Ca^{++} concentration increases: (*a*) negatively-charged chromatin may be bound with Ca^{++} and become increasingly condensed, (*b*) mitochondria would take up large amounts of Ca^{++}, swell osmotically, and uncouple (oxygen consumption is known to increase [2, 39]); 3) Ca^{++} may also be taken up by other smooth membrane compartments, i.e., condensing vacuoles and smooth endoplasmic reticulum, causing osmotic swelling and vacuolation. When Ca^{++} concentrations inside the cell can be returned to within normal ranges, the cell becomes morphologically normal.

The parotid gland appears to be a useful model for studying the effects of elevated cytosolic Ca^{++} on cellular morphology. The possible relationship of these effects to other processes involving stress and to pathological observations is interesting and should be the subject of future investigations.

We thank Dr. Hugo Seibel for furnishing laboratory space in the Department of Anatomy electron microscope facility and Virgil Mumaw for graciously making available the electron microscope in the Department of Pathology. We would also like to express our appreciation to Dr. Linda Sicko-Goad of the Great Lakes Research Institute at the University of Michigan for many fruitful discussions on morphometry and statistical analyses.

This research was supported in part by a grant from the National Institutes of Health (#DE-05764).

Received for publication 10 February 1983, and in revised form 16 May 1983.

REFERENCES

1. Schramm, M., and Z. Selinger. 1975. The functions of cyclic AMP and calcium as alternative second messengers in parotid gland and pancreas. *J. Cyclic Nucleotide Res.* 1:181–192.
2. Schmidt, H.-W., V. Herzog, and F. Miller. 1980. Oxygen consumption of isolated acini from rat parotid gland. *Eur. J. Cell Biol.* 20:201–208.
3. Tapp, R. L., and O. A. Trowell. 1967. The experimental production of watery vacuolation in the acinar cells of the submandibular gland. *J. Physiol. (Lond.)* 188:191–205.
4. Tapp, R. L. 1970. Anoxic and secretory vacuolation in the acinar cells of the pancreas. *Q. J. Exp. Physiol. Cogn. Med. Sci.* 55:1–15.
5. Basbaum, C. B., I. Ueki, L. Brezina, and J. A. Nadel. 1981. Tracheal submucosal gland serous cells stimulated in vitro with adrenergic and cholinergic agonists. A morphometric study. *Cell Tissue Res.* 220:481–498.
6. Mills, J. W., and P. M. Quinton. 1981. Formation of stimulus-induced vacuoles in serous cells of tracheal submucosal glands. *Am. J. Physiol.* 241:C18–C24.
7. Garrett, J. R., and T. J. Harrop. 1978. Reflex influences on watery vacuole formation in parotid acinar cells of rats. *J. Physiol. (Lond.)* 284:86P–87P.
8. Putney, J. W., Jr. 1978. Stimulus-permeability coupling: role of calcium in the receptor regulation of membrane permeability. *Pharmacol. Rev.* 30:209–245.
9. Trump, B. F., I. K. Berezesky, K. U. Laiho, A. F. Osornio, W. J. Mergner, and M. W. Smith. 1980. The role of calcium in cell injury. A review. *Scanning Electron Microsc.* 2:437–462.
10. Quinton, P. M. 1981. Possible mechanisms of stimulus-induced vacuolation in serous cells of tracheal secretory glands. *Am. J. Physiol.* 241:C25–C32.
11. Leslie, B. A., and J. W. Putney, Jr. 1982. Control of vacuole formation in the parotid gland. *40th Annu. Proc. Electron Microsc. Soc. Am.* 166–167.
12. Leslie, B. A., and J. W. Putney, Jr. 1982. Calcium and receptor-mediated vacuole formation in the parotid gland. *J. Cell Biol.* 95 (2, Pt. 2): 242*a*. (Abstr.)
13. Bernfield, P. 1955. Amylases, α and β. *In* Methods in Enzymology. S. P. Colowick and N. O. Kaplan, editors. Academic Press, Inc., New York. 1:49.
14. Spurr, A. R. 1969. A low viscosity epoxy resin embedding medium for electron microscopy. *J. Ultrastruct. Res.* 26:31–43.
15. Millonig, G. 1976. Laboratory Manual of Biological Electron Microscopy. Mario Saviolo, editor. Vercelli, Italy. 1–3.
16. Weibel, E. R., and R. P. Bolender. 1973. Stereological techniques for electron microscopic morphometry. *In* Principles and Techniques of Electron Microscopy. M. A. Hayat, editor. Van Nostrand Reinhold Company, New York. 3:237–296.
17. Williams, M. A. 1977. Quantitative methods in biology. *In* Practical Methods in Electron Microscopy. A. M. Glauert, editor. North-Holland Publishing Co., New York. 6:5–84.
18. Venable, J. H., and R. Coggeshall. 1965. A simplified lead citrate stain for use in electron microscopy. *J. Cell Biol.* 25:407–408.
19. Leslie, B. A., J. W. Putney, Jr., and J. M. Sherman. 1976. α-Adrenergic, β-adrenergic and cholinergic mechanisms for amylase secretion by rat parotid gland *in vitro*. *J. Physiol. (Lond.)* 260:351–370.
20. Young, J. A., and E. W. Van Lennep. 1978. The Morphology of Salivary Glands. Academic Press, Inc., New York.
21. Putney, J. W., Jr. 1978. Role of calcium in the fade of the potassium release response in the rat parotid gland. *J. Physiol. (Lond.)* 281:383–394.
22. Putney, J. W., Jr. 1976. Stimulation of ^{45}Ca influx in rat parotid gland by carbachol. *J. Pharmacol. Exp. Ther.* 199:526–537.
23. Putney, J. W., Jr., C. M. Van De Walle, and B. A. Leslie. 1978. Receptor control of calcium influx in parotid acinar cells. *Mol. Pharmacol.* 14:1046–1053.
24. Peterson, O. H. 1980. The electrophysiology of gland cells. *In* Monographs of the Physiological Society, No. 36. Academic Press, Inc., London.
25. Schramm, M. 1968. Amylase secretion in rat parotid slices by apparent activation of endogenous catecholamine. *Biochim. Biophys. Acta.* 165:546–549.
26. Poggioli, J., B. A. Leslie, J. S. McKinney, S. J. Weiss, and J. W. Putney, Jr. 1982. Action of ionomycin in rat parotid gland. *J. Pharmacol. Exp. Ther.* 221:247–253.
27. Batzri, S., A. Amsterdam, Z. Selinger, I. Ohad, M. Schramm. 1971. Epinephrine-induced vacuole formation in parotid gland cells and its independence of the secretory process. *Proc. Natl. Acad. Sci. USA* 68:121–123.
28. Putney, J. W., Jr., and R. J. Parod. 1978. Calcium-mediated effects of carbachol on cation pumping and Na uptake in rat parotid gland slices. *J. Pharmacol. Exp. Ther.* 205:449–458.
29. Peterson, O. H. 1970. The importance of extracellular sodium and potassium for acetylcholine-evoked salivary secretion. *Experientia.* 26:1103–1104.
30. Selinger, Z., S. Batzri, S. Eimerl, and M. Schramm. 1973. Calcium and energy requirements for K^+ release mediated by the epinephrine α-receptor in rat parotid slices. *J. Biol. Chem.* 248:369–372.
31. Pedersen, G. L., and O. H. Petersen. 1973. Membrane potential measurement in parotid acinar cells. *J. Physiol. (Lond.)* 234:217–227.
32. Landis, C. A., and J. W. Putney, Jr. 1979. Calcium and receptor regulation of radiosodium uptake by dispersed rat parotid acinar cells. *J. Physiol. (Lond.)* 297:369–377.
33. Parod, R. J., and J. W. Putney, Jr. 1980. Stimulus-permeability coupling in rat lacrimal gland. *Am. J. Physiol.* 239:G106–G113.
34. Petersen, O. H., T. A. Gray, and R. A. Hall. 1977. The relationship between stimulation-induced potassium release and amylase secretion in the mouse parotid. *Pfluegers Arch. Eur. J. Physiol.* 369:207–211.
35. Farber, J. L. 1982. Biology of disease. Membrane injury and calcium homeostasis in the pathogenesis of coagulative neurosis. *Lab. Invest.* 47:114–123.
36. Ledger, P. W., N. Uchida, and M. L. Tanzer. 1980. Immunocytochemical localization of procollagen and fibronectin in human fibroblasts: effects of the monovalent ionophore, monensin. *J. Cell Biol.* 87:663–671.
37. Wilcox, D. K., R. P. Kitson, and C. C. Widnell. 1982. Inhibition of pinocytosis in rat embryo fibroblasts treated with monensin. *J. Cell Biol.* 92:859–864.
38. Somlyo, A. P., R. E. Garfield, S. Chacko, and A. V. Somlyo. 1975. Golgi organelle response to the antibiotic X537A. *J. Cell Biol.* 66:425–443.
39. Putney, J. W., Jr. 1978. Oxygen consumption in the parotid gland. *Life Sci.* 22:1731–1736.